Sheffield Hallam University

Electron impact on K+: mechanisms for extreme ultraviolet submission

BERRINGTON, K. A., NAKAZAKI, S. and MURAKAMI, Y.

Available from Sheffield Hallam University Research Archive (SHURA) at:

https://shura.shu.ac.uk/868/

This document is the

Citation:

BERRINGTON, K. A., NAKAZAKI, S. and MURAKAMI, Y. (2006). Electron impact on K+: mechanisms for extreme ultraviolet submission. Journal of physics B: Atomic, molecular and optical physics, 39, 4733-4745. [Article]

Copyright and re-use policy

See http://shura.shu.ac.uk/information.html

Electron impact on K^+: mechanisms for extreme ultraviolet emission

K A Berrington[1], S Nakazaki[2] and Y Murakami[2]
[1]Faculty of Arts, Computing, Engineering and Science,
Sheffield Hallam University, Sheffield, S1 1WB, UK
[2]Department of Applied Physics, Faculty of Engineering,
University of Miyazaki, Miyazaki 889-2192, Japan

August 14, 2006

Abstract

A series of R-matrix calculations on K^+ is used to derive electron excitation and ionization cross sections. The excitation cross section to the $4s$ and $3d$ levels leading to the K^+ 60.1, 60.8 and 61.3nm emission lines shows poor agreement with the cross beam experiment of Zapesochny et al (1986, Zh. Eksp. Teor. Fiz. **90** 1972 [Sov. Phys. JETP **63** 1155]). Cross sections are also presented for exciting the $4p$, $5s$ and $4d$ levels, the autoionizing $3s$ open-shell levels, and for ionization. It is shown how pseudoresonances in the calculated cross section can be eliminated by increasing the target basis.

1 Introduction

In common with other alkali atoms, potassium has a loosely bound outer electron with a low ionization energy (4.34 eV), and becomes easily ionized in a plasma even at relatively low temperatures.

For example in forest fires, where the abundance of potassium can be up to 7% by weight, significant amounts of K^+ could be present at typical hot fire temperatures of 1200K, and may be detected in satellite geo-imaging spectroscopy (Prins et al 1998, Schmit et al 2005). In astrophysical plasmas, potassium is normally a minor constituent because of its low cosmic abundance; however, Reid and Menten (1997) have shown that in the radio photospheres of long-period variable stars, potassium supplies most of the free electrons at temperatures below 1600K.

Although at these low plasma temperatures collisional excitation is relatively unimportant, it should be noted that the ionization energy of K^+ is over seven times greater than that of K, so K^+ will persist over a large temperature range, contributing to opacity and providing plasma diagnostics.

From the atomic physics point of view, K^+ is interesting because it is the atomic system which shows the closest degeneracy of an outer $4s$ and $3d$ electron, and therefore involves closely-coupled excitation channels with strong inter

and intra shell correlations. The lowest excited states lie close together, as do their spectral emission lines resulting from decays to the ground state, making this a useful system for spectral diagnostics.

As with other sytems with completely filled shells, K^+ has a large energy difference between the ground and excited states ($\sim$20eV). Emission lines from K^+ therefore lie in the interface between the ultraviolet and X-ray spectral region at around 60nm. In this region, the strongest lines in the potassium spectrum are from decays to the K^+ ground level $3s^23p^6\ ^1S_0$ from $3s^23p^53d$ $^1P_1^o$ at 49.5nm, $3s^23p^54s\ ^1P_1^o$ at 60.1nm, $3s^23p^53d\ ^3P_1^o$ at 60.8nm, $3s^23p^54s$ $^3P_1^o$ at 61.3nm, together with $3s3p^6\ ^2S_{1/2} \rightarrow 3s^23p^5\ ^2P_{1/2}^o$ in K^{2+} at 77.9nm.

The last four lines, and similar ones in other alkali metal ions, were studied in a cross beam experiment by Zapesochny et al (1986) to determine the energy dependence of the corresponding excitation functions, and they reported a pronounced resonance structure and a rather large excitation cross section for K^+ of the order of 10^{-16} cm^2 in the near threshold region. To our knowledge, these results have not been verified since; in particular there does not seem to have been an independent theoretical calculation to account for these findings, and this provides a motivation for the current work.

At shorter wavelengths (44–47nm), lines arise from transitions to ground state from $3p^55s$ and $3p^54d$. Further strong lines of K^+ occur in the optical spectrum near 420nm, arising from excitations of the $3p^54p$ states followed by $4p \rightarrow 4s$ and $4p \rightarrow 3d$ radiative decay. As a by-product of our investigations we can quantify the cross section to these states also.

An accurate calculation of the excitation of the potassium lines requires us also to consider the electron impact ionization cross section. Hirayama (1987) measured the ionization cross section for K^+ with good accuracy, so this provides an important benchmark for our calculation.

2   The calculations

The R-matrix method and programs (Berrington et al 1995) are used to quantify the cross section to the excited levels of K^+, particularly those levels that are responsible for the emission lines, $3s^23p^6$, $3s^23p^54s$, $3s^23p^53d$, $3s^23p^54p$, $3s^23p^54d$ and $3s^23p^55s$. The main scattering calculation uses a 36 term (66 fine structure levels) intermediate-coupling frame transformation R-matrix (icfRM) method, but we also examine a 27 level Breit-Pauli R-matrix (BPRM) calculation to confirm that relativistic effects are adequately accounted for, and some LS coupling calculations with different numbers of target terms to elucidate the origin of pseudoresonance effects in the ionization cross section, as described below.

The primary output from our calculation is the collision strength matrix $\Omega(E)$, from which we derive the cross section

$$Q_{i \rightarrow j}(E) = \Omega_{ij}\pi a_0^2/(gE) \tag{1}$$

where E is the initial electron energy in Rydbergs (13.6057 eV), g is the statistical weight of the initial state i, and $a_0 = 5.29177 \times 10^{-9}$ cm, the Bohr

radius.

Because of the paucity of published work on this ion, we carry out a series of test calculations as well as the main calculation to compare and contrast different approaches. These include varying the orbital basis, the size of the close-coupling expansion employed and the way relativistic effects are included, as described below.

2.1 The K$^+$ target expansion (36 terms, 66 levels)

We use the $1s, 2s, 2p, 3s, 3p$ one-electron radial orbitals for the Ar-like K ion ground state from Clementi and Roetti (1974). We augment these with excited orbitals $4s, 5s, 4p, 3d, 4d$ and pseudo orbitals $\bar{d}$ and $\bar{f}$ generated from Hibbert's (1975) variational program CIV3 in the following way: $4s, \bar{d}$ and $\bar{f}$ optimised on the lowest $^3P^{\mathrm{o}}$ term in the CI mixture, $3p^5 4s + 3p^5 3d + 3p^4(^1D)4s\bar{f} + 3p^4 3d\bar{f} + 3p^5\bar{d}$; $3d$ optimised on the second $^3P^{\mathrm{o}}$ term, $3p^5 3d$; $5s$ optimised on the third $^3P^{\mathrm{o}}$ term, $3p^5 5s$; $4d$ optimised on the fourth $^3P^{\mathrm{o}}$ term, $3p^5 4d$; $4p$ optimised on $3p^5 4p\ ^3D$.

These orbitals, orthonormalized for each angular momentum, are defined analytically in table 1. A configuration interaction wavefunction is used to describe the target state wavefunction ψ_i, described by an antisymmetrised expansion in N-electron configurations ϕ_j with coefficients a_{ij}, which diagonalizes the N-electron Hamiltonian H^N with eigenergies E_i,

$$\psi_i(\mathbf{r}_1 \ldots \mathbf{r}_N) = \sum_j a_{ij}\phi_j(\mathbf{r}_1 \ldots \mathbf{r}_N), \quad (\psi_i|H^N|\psi_{i'}) = E_i \delta_{ii'} \tag{2}$$

We use all important configurations ϕ_j with a $3s^2 3p^3$ or $3s3p^4$ core, only excluding those whose normalised eigenvector components contribute less than 0.001 for the terms included. This saves time in the calculation by reducing the total number of N electron configurations from 20426 to 6275, 2257 even parity and 4018 odd parity, without affecting the results. We include Breit-Pauli operators in the Hamiltonian, with Blume and Watson (1963) screening. The calculated energy levels are compared in tables 2 and 3 with experimental where possible.

The 36 term (66 level) icfRM target level energies are tabulated in tables 2 and 3, and are in good overall agreement with experiment where available. The first 42 levels correspond to physical states, above which there is a mixture of continuum states and pseudostates: the ionization threshold occurs after level 52, and the remaining 14 levels contribute to ionization. There is a systematic discrepency with experiment for the $3s3p^6 nl$ energies probably because we do not correct sufficiently for the different $3s$ orbital.

The calculated oscillator strengths for transitions involving the ground and first metastable level are shown in table 4. The length and velocity forms from the 36 term icfRM calculations lie within the experimental error bars for the $^1S_0^{\mathrm{e}} \rightarrow \ ^{3,1}P_1^{\mathrm{o}}$ 1–3, 1–5 and 1–8 transitions. However, our results do not agree well with the relativistic configuration interaction (RCI) Dirac-Fock calculation of Beck (2002), particularly for 1–3, where he has a value twice that of experiment. Beck points out that his summed oscillator strength to levels 3, 5 and 8 (0.461) is close to experiment (0.469), whereas ours is perhaps too high

0.515. His calculation is similar to ours in the configuration expansion used, but he includes relativistic effects more completely with the Dirac approach, and his energy levels are in better agreement with experiment. Pragmatically, we have to agree to differ on the oscillator strengths in order to carry out our aim of a computationally feasible collision calculation with a wide range of target and continuum states.

For oscillator strengths involving excited levels, for example from the $^3P_2^o$ level 2 as shown in table 4, our results tend to be greater than those calculated by Smirnov and Shapochkin (1979) from lifetime measurements.

2.2 The icfRM scattering expansion

The R-matrix method considers the scattering wavefunction in two regions, whose boundary is a sphere of sufficient size to enclose the N-electron target states ψ_i (in our case 26.6 a_0). In the internal region we write the wavefunction as an antisymmetrised sum over products of ψ_i and the scattering electron function u_j coupled to channel i, together with a sum over $N+1$ electron configurations $\Phi_j(\mathbf{r}_1 \ldots \mathbf{r}_{N+1})$ required by orthogonality,

$$\Psi_k(\mathbf{r}_1 \ldots \mathbf{r}_{N+1}) \;\; = \;\; \sum_{ij} c_{ijk}\psi_i u_j + \sum_j d_{jk}\Phi_j \tag{3}$$

where the c_{ijk} and d_{jk} coefficients are chosen to diagonalize the $N+1$ electron Hamiltonian.

The ψ_i basis consists of bound target terms, together with pseudostates associated with the $\bar{d}$ pseudo-orbital which span the ionization threshold, and autoionizing states in the continuum. This is shown in figure 1. This is equivalent to rewriting the R-matrix basis in (3) as a sum over bound states ψ_i^B (levels 1–42), bound pseudostates $\bar{\psi}_i^B$ (levels 43–52), continuum pseudostates $\bar{\psi}_i^C$ (levels 53–55) and continuum states ψ_i^C (levels 56–66). We will make use of $\bar{\psi}_i^C$ and ψ_i^C to extract ionization cross sections. For the Φ_j in the scattering expansion we include all configurations with a $3s^2 3p^4$ or $3s 3p^5$ core.

The term-coupling transformation uses the R-matrix method in conjunction with the intermediate-coupling frame transformation method (Griffin et al 1998). The one-electron mass correction and Darwin terms are included in the Hamiltonian, and the external region equations are solved in LS coupling. Use is made of multichannel quantum defect theory (MQDT) to obtain 'unphysical' collision matrices as implemented by Gorczyca and Badnell (2000) in the computer code STGICF. The outer region solutions include the long-range coupling potentials as a perturbation, still within the MQDT framework (Gorczyca et al 1996, Badnell and Seaton 1999). We apply a 'top-up' in total angular momentum at $J = 14.5$, and 60 continuum functions per channel enable us to reach a scattering energy of 400eV.

Because the computational effort in close-coupling and R-matrix methods depends critically on the number of coupled channels, and there are fewer channels for a given term expansion in LS coupling than in intermediate coupling, then this is normally a much faster procedure than a fully relativistic procedure,

without losing much accuracy. This speed-up enables us to include the extra target terms and correlation as described above.

2.3 The 27 level BPRM test calculation

We also examine a 27 level Breit-Pauli R-matrix (BPRM) calculation to confirm that relativistic effects are adequately accounted for. In this calculation, relativistic effects are incorporated via terms of the Breit-Pauli Hamiltonian, including explicitly the one-electron mass correction and Darwin terms and the spin-orbit interaction; implicitly accounted for are fine-structure two-electron contributions from closed subshells from closed subshells (Berrington et al 1995). A recoupling transformation is applied to the LS-coupled Hamiltonian matrices in the internal region, and the external region equations are solved in the intermediate coupling scheme to give fine-structure cross sections directly. For an ion like K^+, the Breit-Pauli approach is essentially equivalent to a fully relativistic Dirac Hamiltonian approach (Berrington et al 2005).

We do not include $5s$, $4d$ and $\bar{f}$ target orbitals in BPRM. The 27 levels ψ_i included are all those from $3s^2 3p^6$ and $3s^2 3p^5 nl$ configurations, with nl as $4s$, $3d$ and $4p$. These are represented by 98 target configurations ϕ_j, focused on an accurate representation of the lowest $^1S^e$ and $^{1,3}P^o$ terms by including configurations $3s^2 3p^5 nl$, together with contributions from $3s^2 3p^4(4s^2, 4s3d, 3d^2)$ for $^1S^e$ and $3s^2 3p^4(4s4p, 3d4p)$, $3s^2 3p^3(4s^2 3d, 4s3d^2, 3d^3)$ and $3s3p^5(3d^2, 4s3d, 4s\bar{d})$ for $^{1,3}P^o$. The $N+1$ electron configurations Φ_j in the scattering expansion includes those configurations with a $3s^2 3p^5$ core. For the low energies of interest, we include twenty continuum functions u_j per channel, and partial waves are calculated for total angular momentum $J \leq 10.5$.

Table 5 shows the target energies and oscillator strengths from the 27 level BPRM calculation. The energies are not so good because of its more limited CI expansion than in icfRM. The length and velocity forms of the oscillator strengths lie within the experimental error bars for the $^1S_0^e \rightarrow {}^{3,1}P_1^o$ 1-3, 1-5 and 1-8 transitions, the oscilator strength sum (0.465) is close to experiment, and there is qualitative consistency between our 27 level BPRM and 36 term icfRM calculations.

3 The cross sections

Figure 2 presents the cross section from the 36 term icfRM calculation for excitations out of the $J = 0^e$ ground state to levels 2 ($J = 2^o$), 3, 5 and 8 ($J = 1^o$), together with the cross section summed over all the $3s^2 3p^5 4p$ levels and all the $3s3p^6 nl$ levels. Resonant effects appear to be confined to the near threshold region for the lower levels.

Table 2 also presents the collision strength from the ground state in the 36 term icfRM calculation to the physical bound levels ψ_i^B.

3.1 Excitation for the 60.1, 60.8 and 61.3nm lines

In the top frame of figure 2 we plot the summed excitation of the 3, 5 and 8 levels, $^1S_0^{\mathrm{e}} \rightarrow {}^{3,1}P_1^{\mathrm{o}}$, convolved over a 1 eV Gaussian to simulate the energy nonuniformity of the electron beam used by Zapesochny et al (1986). Theirs was a crossed electron-ion beam experiment, in which the cross sections were deduced by variations with respect to electron energy in the emission produced by radiative decay $^{3,1}P_1^{\mathrm{o}} \rightarrow {}^1S_0^{\mathrm{e}}$ of levels 3, 5 and 8 (they were unable to resolve the individual lines). They normalised their cross section to a Coulomb-Born calculation on Rb^+ at 400 eV. In our icfRM calculation, we find a cross section for K^+ at 400 eV four times smaller than that given by Zapesochny et al, so in our figures we reduce their measurements by this factor. Although they give several sources of error in their experiment which cumulatively add up to 100%, this factor of 4 descrepancy with our calculation indicates the need for further investigation.

In figure 3 we show detail of the low energy behaviour of the measurements, together with our icfRM calculation, and there is little agreement between the two in either magnitude or structure. Figure 3 also compares the BPRM calculation with and without the $\bar{d}$ orbital for the summed excitation of the 3, 5 and 8 levels, $^1S_0^{\mathrm{e}} \rightarrow {}^{3,1}P_1^{\mathrm{o}}$, showing that for these transition the $\bar{d}$ has little effect. The BPRM and icfRM comparison, which represents two different R-matrix approaches, shows the persistence of the discrepancy between theory and experiment. We comment further on the Zapesochny et al structures in subsection 3.4.

3.2 Convergence of excitation cross sections

Although the BPRM and icfRM cross sections are similar for the low-lying transitions, there are serious differences between the models for excitation of higher states of K^+, in particular $3s^2 3p^6\ ^1S^{\mathrm{e}} \rightarrow 3s^2 3p^5 3d\ ^1P^{\mathrm{o}}$ (the final state being the 15th term and 27th level). Figure 4 shows this cross section from three 15 term calculations, which involve only the bound states ψ_i^B, compared with the 36 term calculation. The curve labelled '15($3p^5$)' is the 15 term LS coupling calculation corresponding to the 27 level BPRM calculation where only those $N+1$ electron configurations are included with a $3s^2 3p^5$ core, and shows a large pseudoresonance at 35 eV. This is also present in the curve labelled '15', which is also a 15-term calculation, but uses the full set of $N+1$ electron configurations included in the 36 term calculation. The pseudoresonance is not present when the $\bar{d}$ orbital is not included (the curve labelled '15(no $\bar{d}$)', so we assume the pseudoresonance arises from including $\bar{d}$ in the target and $N+1$ electron configurations, but not explicitly as a target state. This is confirmed by the 36 term calculation, which allows for loss of flux to target states involving the $\bar{d}$, and shows no sign of the pseudoresonance.

The common characteristic of the 15 term calculations shown here is that they exlude the loss of flux to the continuum and so grossly overestimate the cross section to the 15th term (and also to a lesser extent to other terms) around the ionization threshold. By contrast the 36 term icfRM calculation appears to

be well converged for the excitation of the lower states.

3.3 Convergence of electron impact ionization

One purpose of the extra terms included in the 36 term icfRM calculation, as opposed to the BPRM calculation, is to account for ionization channels. The ionization cross section can be extracted simply by summing the excitation cross section to all the continuum target states $\bar{\psi}_i^C$ and ψ_i^C. This is shown in figures 5a and 5b, and it agrees well with the experiment of Hirayama (1987).

However, the 36 term calculation of the ionization cross section is affected by pseudoresonances at scattering energies 45-70 eV. As in the previous subsection, we attribute this to a mismatch in the N-electron target and $N + 1$ electron scattering system correlation. To explore this further, we look at the dominant partial wave for ionization, $^2G^{\mathrm{e}}$, and find that pseudoresonances around 55-60eV arise from $3s^23p^43d^2nd$ configurations in the $N + 1$ electron configurations Φ_j. This indicates that the close-coupling expansion is missing some contributions in the 36 term expansion. So, taking the same configuration-interaction target expansion of the icfRM calculation, which contains 6275 configurations, we augment the target expansion with further continuum states ψ_i^C up to a total of 120 terms. In figure 5b we show that the resulting $^2G^{\mathrm{e}}$ partial ionization cross section (the dashed line labelled G) is much smoother than the 36 term one, The resulting 120-term calculation brings in many doubly-excited terms arising from $3s^23p^44s4l$ and $3s^23p^43d4l$: all these lie in the continuum and span the pseudoresonance region up to 53.65 eV. 24 continuum functions per channel are included, as we only apply this calculation to scattering energies below 120eV. A similar feature occurs in the $^2H^{\mathrm{o}}$ partial wave, as shown in figure 5b; again we attribute the oscillations around 130 eV to limitations of the target expansion.

Table 3 also presents the 36 term icfRM collision strength summed over levels 53 and above, which lie in the continuum, representing the ionization collision strength. Levels 40–49 are $3s3p^6nl$ innershell excited states, defined in table 3, and represent physical states ψ_i^C in the continuum. The innershell collision strength contributes up to a third of the total for ionization at the lower energies shown in figure 5a, but much less at higher energies as can be seen in table 3. This indirect ionization process gives rise to structures around the innershell thresholds; for example, the hump in the ionization cross section at 40 eV, visible in figure 5a, is due to excitation of $3s3p^63d$.

In our calculation the transition responsible for nearly all the direct ionization is the excitation of pseudo level 55, $3s^23p^5\bar{d}\,^1P_1^{\mathrm{o}}$, whose threshold is at 32.38 eV, and channels $\epsilon p\,^2D^{\mathrm{e}}$ and $\epsilon f\,^2G^{\mathrm{e}}$ contribute most of the near-threshold cross section. It is fortuitous that our choice of $\bar{d}$, a correlation orbital, should give a good account of ionization. Although we have pseudostates lying both below and above the ionization threshold, no attempt has been made here to vary the pseudo-orbital basis to examine its convergence. So we do not claim our calculated ionization cross section is anything other than a good estimate, as can be seen in figure 5 by comparison with the experiment of Hirayama (1987). Rather, we claim to have made a reasonable allowance for continnum effects to improve our calculation of excitation cross sections in the intermediate energy

region.

3.4   Structures in the cross section

The cross section of Zapesochny et al (1986) has pronounced structure, in particular three narrow peaks near threshold and a broad gentle maximum at around 40 eV. However, apart from the first peak at threshold, we cannot reproduce these features by consideration of excitation of the $^{3,1}P_1^{\rm o}$ levels 3, 5 and 8 alone, as can be seen in figure 2.

The identification of these three narrow peaks by Zapesochny et al seems however to be sound: the first peak being due to resonance lines originating from the levels of the d configuration, the second peak being due to excitation of the (even parity) $3s^23p^54p$ levels followed by radiative cascade to the (odd parity) 3, 5 and 8 levels, and the third peak being due to autoionizing states converging to highly excited levels. Figure 2 indicates broad agreement with the first two peaks, but we cannot investiage the third because we do not have such (bound) states in our calculation.

The broad maximum around 40 eV in the experiment is difficult to explain, though we note that this coincides with the onset of excitation to the $3s3p^6nl$ levels in the continuum.

One of the most striking features we find is a large $^2D^{\rm e}$ resonance near 35 eV in the 1-8 transition, $3s^23p^6\ ^1S_0^{\rm e} - 3s^23p^54s\ ^1P_1^{\rm o}$. This is shown in the cross section in figure 6, where we also plot the $^2D^{\rm e}$ partial wave contribution responsible for the resonance. This is an interesting 2-electron process caused by $3s$ innershell excitation accompanied by simultaneous capture of the incoming d electron, followed by a $3p \rightarrow 3s$ relaxation and ejection of an electron:

$$\mathrm{e}^- + 3s^23p^6\ ^1S^{\rm e} \rightarrow (3s3p^64s3d)^2D^{\rm e} \rightarrow 3s^23p^54s\ ^1P^{\rm o} + \mathrm{e}^-. \qquad (4)$$

An analysis of this resonance using the QB method (Quigley and Berrington 1996, Quigley et al 1998), which locates resonances at the maxima of the eigenphase sum derivative, identifies the resonance at 35.6 eV, attributable to the $3s3p^64s3d\ ^2D^{\rm e}$ configuration, with a width of 0.17 eV. This resonance is the lowest of the Rydberg series converging onto the $3s3p^64s\ ^3S^{\rm e}$ target term, and table 3 shows our calculated energies of the innershell states may be too high by 1 eV compared with experiment (Aizawa et al 1985), so we refer to this resonance as 'near 35 eV' to reflect the uncertainty in energy.

The $^2D^{\rm e}$ resonance also affects other transitions, for example figure 5a shows the resonance as a dip in the ionization cross section near 35 eV. Here the resonant state in (4) decays through $3p \rightarrow 3s$ relaxation accompanied by two electron emission, $(3s3p^64s3d)^2D^{\rm e} \rightarrow 3s^23p^5\ ^2P^{\rm o} + 2\mathrm{e}^-$.

Apart from narrow resonances near threshold, and the large resonance near 35 eV, we find little structure in the cross section, in contrast to Zapesochny et al, and our background cross section for exciting the $J = 1^{\rm o}$ levels (3+5+8) of 2×10^{-17} cm^2 in the 40–50 eV region is an order of magnitude below theirs, where they predict a maximum. A possible reason why Zapesochny et al observe a large emission cross section could be that there were other mechanisms for populating the $J = 1^{\rm o}$ levels in their experiment apart from direct excitation.

For example, the cross section to $3p^5 4p\,^1 S_0$ (level 26) is comparable to that of $3p^5 4s\,^1 P_1^{\mathrm{o}}$ (level 8, see table 2). Since the radiative lifetime between these levels is only about 3 ns, it is conceivable that excitation of the $4p$ level followed by radiative decay to the $4s$ level would enhance the latter's 60.1nm emission.

4 Conclusion

Cross sections for electron excitation of K^+ are presented in a series of R-matrix calculations, which include both relativistic (at the Breit-Pauli level) and non-relativistic approaches, and different numbers of target states. The overall agreement between these methods is good, once allowance has been made for truncating the target state expansion, and we have shown how pseudoresonances in the calculations can be ameliorated by increasing the target basis. However, the experiment by Zapesochny et al (1986) is difficult to interpret with our results: their magnitude of the $^1 S_0^{\mathrm{e}} - {}^{3,1} P_1^{\mathrm{o}}$ cross section is at least four times higher than ours, and we find different structures. For example, apart from the near-threshold peak, the other peaks are probably due to radiative cascade from higher states. We do though find a large $^2 D^{\mathrm{e}}$ resonance in the $^1 S_0^{\mathrm{e}} - {}^1 P_1^{\mathrm{o}}$ cross section, and predict that this same resonance should appear in the ionization cross section.

Our ionization cross section should be good in the 33-43 eV energy range: we predict a change of gradient at 37 eV due to the onset of innershell excitation, and estimate that the innershell contribution can be up to a third of the total for ionization. As far as we are aware, this is the first time that resonance structure and the innershell contribution in the ionization cross section has been quantified for K^+.

We have tabulated the excitation and ionization collision strengths from our calculation, including those for the $3s$ hole states, to aid in future work.

Acknowledgements

References

Aizawa H, Wakiya K, Suzuki H, Koike F and Sasaki F 1985 *J. Phys. B: At. Mol. Opt. Phys.* **18** 289

Aymar M and Schweighofer M G 1973 *Physica* **67** 585

Beck D R 2002 *J. Phys. B: At. Mol. Opt. Phys.* **35** 4155

Berrington K A, Eissner W B and Norrington P H 1995 *Comput. Phys. Commun.* **92** 290

Berrington K A, Ballance C P, Griffin D C and Badnell N R 2005, *J. Phys. B: At. Mol. Opt. Phys.* **38** 1667

Badnell N R and Seaton M J 1999 *J. Phys. B: At. Mol. Opt. Phys.* **32** 3955

Blume M and Watson R E 1963 *Proc. R. Soc.* A **271** 565

Clementi E and Roetti C 1974 *Atom. Data Nucl. Data Tables* **14** 177

Gorczyca T W and Badnell N R 2000 *J. Phys. B: At. Mol. Opt. Phys.* **33** 2511

Gorczyca T W, Robicheaux F, Pindzola M S and Badnell N R 1996 *Phys. Rev.* A **54** 2107

Griffin D C, Badnell N R and Pindzola M S 1998 *J. Phys. B: At. Mol. Opt. Phys.* **31** 3713

Henderson M, Curtis L J, Matulioniene R, Ellis D G, Li Y 1997 *Phys. Rev.* A **55** 2723

Hibbert A 1975 *Comput. Phys. Commun.* **9** 141

Moore C E 1971 *Atomic Energy Levels* NBS Circular No.467, vol 1 (Washington DC: US Government Printing Office) p 230

Quigley L and Berrington K A 1996 J. Phys. B: At, Mol. Opt. Phys. **29** 4529

Quigley L, Berrington K A and Pelan J C 1998 Comput. Phys. Commun. **114** 225

Hirayama T 1987 PhD thesis, Sophia University, Japan; http://www.ne.rikkyo.ac.jp/ hirayama/Lab/Work/eMisc/D-ron/

Prins E M, Feltz J M, Menzel W P and Ward D E 1998 J. Geophys. Res. **103** 31 821

Reid M J and Menten K M (1997) Astrophys J. **476** 327

Schmit T J, Gunshor M M, Menzel W P, Li J, Bachmeier S, Gurka JJ 2005 Bull. Amer. Meteor. Soc.i **8** 1079

Smirnov Yu M and Shapochkin M B 1979 Opt. Spectroc. (USSR) **47** 6

Zapesochny A I, Imre A I, Aleksakhin I S, Zapesochny I P and Zatsarinny O I 1986 Zh. Eksp. Teor. Fiz. **90** 1972 [Sov. Phys. JETP **63** 1155]

Table 1: Radial orbital coefficients, $P_{nl}(r) = \sum_i c_i r^i \exp(-\zeta_i r)$, orthogonalized to the Clementi and Roetti (1974) $1s, 2s, 2p, 3s, 3p$ orbitals for K^+.

| nl	i	ζ_i	c_i	nl	i	ζ_i	c_i
$4s$	1	14.95227	5.446877	$4p$	2	7.79083	18.94905
	2	6.35034	-21.81276		3	2.82795	-4.99807
	3	3.33899	11.58501		4	0.98983	0.10925
	4	1.21193	-0.27378	$3d$	3	1.27918	0.73596
$5s$	1	14.58918	2.70335		3	6.84671	0.75792
	2	6.60615	-11.44923		3	3.19341	9.88608
	3	3.18992	5.14091	$4d$	3	0.52684	0.77300
	4	1.26493	-0.20011		4	1.09984	-1.12092
	5	0.71019	0.00413		5	0.67067	-0.03415
$\bar{f}$	4	2.68	9.51659	$\bar{d}$	3	2.25084	2.60940
					4	0.66130	-0.01714
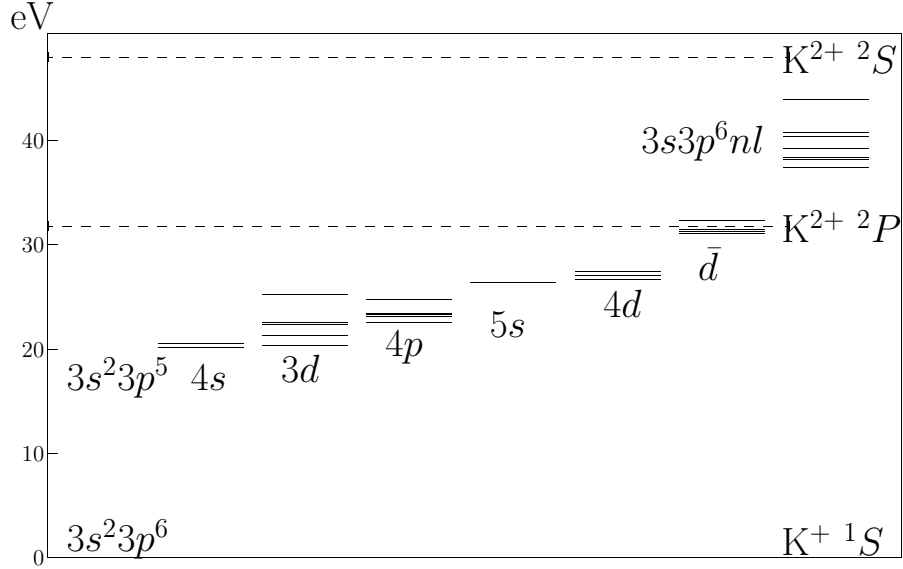
Figure 1: Term energy diagram (calculated energies in eV) showing the 36 K^+ terms included in the icfRM calculation. Dashed lines indicate the K^{2+} ionization thresholds, $3s^2 3p^5\ ^2P$ and $3s3p^6\ ^2S$.

11

Table 2: Energies of the 42 bound levels from the 66-level icfRM calculation for K$^+$, compared with observed values (Aymar and Schweighofer 1973, Moore 1971, http://physics.nist.gov/). The level index i specified here is used as a level identifier in this paper. Also shown is the calculated collision strength from the ground state of K$^+$ to each excited level.

i	Level		Energy (eV)		Collision strength				
			icfRM	Observed	25 eV	50 eV	100 eV	200 eV	400 eV
1	$3p^6$	$^1S_0$	0	0					
2	$3p^54s$	$^3P_2^o$	20.130	20.148	0.1357	0.0918	0.0269	0.0062	0.0013
3		$^3P_1^o$	20.197	20.239	0.1506	0.1156	0.0801	0.0836	0.1139
4	$3p^53d$	$^3P_0^o$	20.208	20.264	0.0717	0.0471	0.0192	0.0058	0.0014
5		$^3P_1^o$	20.391	20.395	0.1706	0.1632	0.2017	0.2846	0.4175
6		$^3P_2^o$	20.424	20.449	0.3855	0.2544	0.1107	0.0341	0.0087
7	$3p^54s$	$^3P_0^o$	20.461	20.476	0.0332	0.0221	0.0083	0.0023	0.0006
8		$^1P_1^o$	20.645	20.639	0.1210	0.4642	1.1681	1.9648	2.9765
9	$3p^53d$	$^3F_4^o$	21.164		0.3563	0.1802	0.0930	0.0260	0.0063
10		$^3F_3^o$	21.251	21.181	0.2970	0.1406	0.0733	0.0220	0.0073
11		$^3F_2^o$	21.327	21.267	0.2266	0.1005	0.0516	0.0144	0.0035
12		$^3D_2^o$	22.400		0.1251	0.1566	0.0361	0.0071	0.0020
13		$^3D_3^o$	22.458		0.0840	0.1063	0.0838	0.0924	0.1110
14		$^1D_2^o$	22.540		0.0631	0.0579	0.0193	0.0029	0.0005
15		$^3D_1^o$	22.547	22.374	0.0334	0.0314	0.0145	0.0087	0.0114
16		$^1F_3^o$	22.617		0.0927	0.1932	0.2236	0.3031	0.3733
17	$3p^54p$	$^3S_1$	22.650	22.715	0.0772	0.0442	0.0206	0.0040	0.0011
18		$^3D_3$	23.058	23.109	0.1667	0.0715	0.0104	0.0027	0.0008
19		$^3D_2$	23.102	23.146	0.0997	0.0656	0.0479	0.0542	0.0431
20		$^3D_1$	23.194	23.251	0.0679	0.0375	0.0053	0.0014	0.0004
21		$^1D_2$	23.290	23.328	0.0790	0.0797	0.1182	0.1443	0.1165
22		$^1P_1$	23.399	23.463	0.0588	0.0642	0.0081	0.0022	0.0007
23		$^3P_2$	23.458	23.515	0.0621	0.0404	0.0471	0.0520	0.0419
24		$^3P_0$	23.497	23.529	0.0120	0.0055	0.0082	0.0081	0.0085
25		$^3P_1$	23.516	23.574	0.0392	0.0234	0.0059	0.0008	0.0002
26		$^1S_0$	24.752	24.149?	0.1202	0.3852	0.9589	1.1373	1.1892
27	$3p^53d$	$^1P_1^o$	25.314	25.040		0.7348	2.4684	4.4184	6.9141
28	$3p^55s$	$^3P_2^o$	26.270	26.356		0.0500	0.0057	0.0007	0.0002
29		$^3P_1^o$	26.331	26.408		0.0831	0.0761	0.1086	0.1368
30		$^3P_0^o$	26.504	26.623		0.0105	0.0012	0.0002	0.0000
31		$^1P_1^o$	26.555	26.659		0.1039	0.1024	0.1480	0.1902
32	$3p^54d$	$^3P_0^o$	26.765			0.0130	0.0040	0.0014	0.0003
33		$^3P_1^o$	26.798	26.707		0.0405	0.0150	0.0093	0.0086
34		$^3P_2^o$	26.860	26.763		0.0687	0.0201	0.0067	0.0016
35		$^3F_4^o$	26.969			0.0883	0.0263	0.0067	0.0016
36		$^3F_3^o$	27.042			0.0712	0.0219	0.0077	0.0049
37		$^3F_2^o$	27.114	26.913		0.0540	0.0142	0.0035	0.0008
38		$^3D_3^o$	27.371	26.995		0.1091	0.0315	0.0285	0.0359
39		$^1D_2^o$	27.421			0.0952	0.0134	0.0024	0.0005
40		$^3D_1^o$	27.485			0.0477	0.0117	0.0123	0.0165
41		$^3D_2^o$	27.492	27.177		0.0820	0.0099	0.0016	0.0003
42		$^1F_3^o$	27.533			0.1075	0.0459	0.0479	0.0615

Table 3: Energies of the $3s$ hole states included in the 36 term icfRM calculation for K$^+$, compared with observed values (Aizawa et al 1985). Also shown is the calculated collision strength from the ground state of K$^+$ to each level. The level indexing i continues from table 2. Note, levels 43-55 are omitted from this table: they range from 31.1–32.4 eV and are associated with $3s^2 3p^5 \bar{d}$ pseudostates. The ionization threshold K$^{2+}(3s^2 3p^5)$ is at 31.6284 eV and collision strengths to levels above this (level 53 and above) are summed for ionization in the row labelled K^{2+}.

i	Level		Energy (eV)		Collision strength			
			icfRM	Aizawa et al	50 eV	100 eV	200 eV	400 eV
56	$3s3p^6 4s$	$^3S_1$	37.44		0.0250	0.0031	0.0010	0.0003
57		$^1S_0$	38.18	36.91±0.1	0.1151	0.1694	0.2051	0.2150
58	$3s3p^6 3d$	$^3D_1$	38.39		0.0693	0.0260	0.0082	0.0021
59		$^3D_2$	38.40		0.1155	0.0434	0.0137	0.0036
60		$^3D_3$	38.41		0.1616	0.0607	0.0191	0.0050
61		$^1D_2$	39.24	38.22±0.1	0.1152	0.3309	0.4649	0.5878
62	$3s3p^6 4p$	$^3P^o_0$	40.42		0.0061	0.0012	0.0002	0.0001
63		$^3P^o_1$	40.43		0.0185	0.0037	0.0008	0.0002
64		$^3P^o_2$	40.44		0.0311	0.0061	0.0012	0.0003
65		$^1P^o_1$	40.78	39.64±0.1	0.0748	0.1246	0.1544	0.1785
66	$3s3p^6 5s$	$^1S_0$	43.94	41.34±0.1	0.0279	0.0459	0.0582	0.0593
K^{2+}					3.11	7.99	12.42	16.77

Table 4: Oscillator strengths for K$^+$ for transitions involving the ground $^1S_0$ and first metastable level $^3P^o_2$: comparisons of the 36 term icfRM calculation with experiment (Henderson et al 1997) and others. The transition is specified by the initial and final level as defined in table 2.

Transition	icfRM(L)	icfRM(V)	Expt	Others
1-3	0.022	0.018	0.020±0.004	0.042[a]
1-5	0.076	0.066	0.069±0.012	0.065[a]
1-8	0.417	0.365	0.38±0.04	0.354[a]
1-15	0.002	0.002		0.004[a]
1-27	1.321	0.983		1.612[a]
2-17	0.160	0.162		0.052[b]
2-18	0.440	0.399		0.121[b]
2-19	0.092	0.084		0.033[b]
2-20	0.017	0.015		0.019[b]
2-21	0.118	0.103		0.041[b]
2-22	0.003	0.002		0.006[b]
2-23	0.041	0.035		0.026[b]
2-25	0.024	0.020		0.012[b]

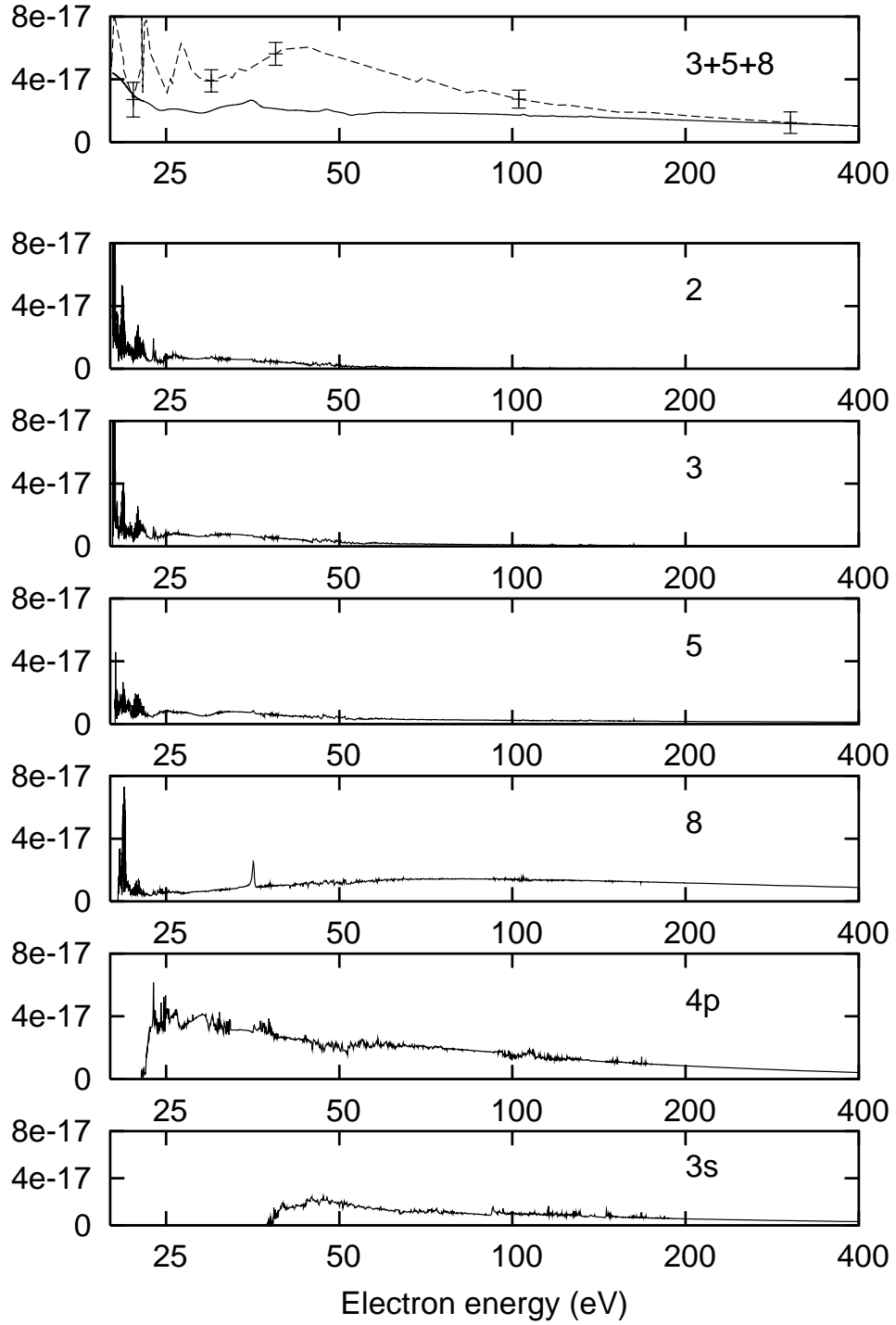[a]Beck (2002); [b]Smirnov and Shapochkin (1979)

Figure 2: Excitation cross section in cm^2 from the ground state of K$^+$ in the icfRM calculation. Top frame: —, $^{3,1}P_1^o$ levels 3,5,8 summed and convolved over a 1 eV Gaussian; - - - -, Zapesochny et al (1986) reduced by a factor of 4. Other frames: excitation to levels 2, 3, 5, 8, $3s^23p^54p$ summed, $3s3p^6nl$ summed.

Table 5: BPRM calculation energies and oscillator strengths for K$^+$ for $^1S_0 - {}^{3,1}P_1^o$ transitions: The transition is specified by the initial and final level as defined in table 2.

Transition	Energy (eV)	BPRM(L)	BPRM(V)
1-3	20.450	0.018	0.016
1-5	20.734	0.073	0.072
1-8	20.948	0.374	0.367
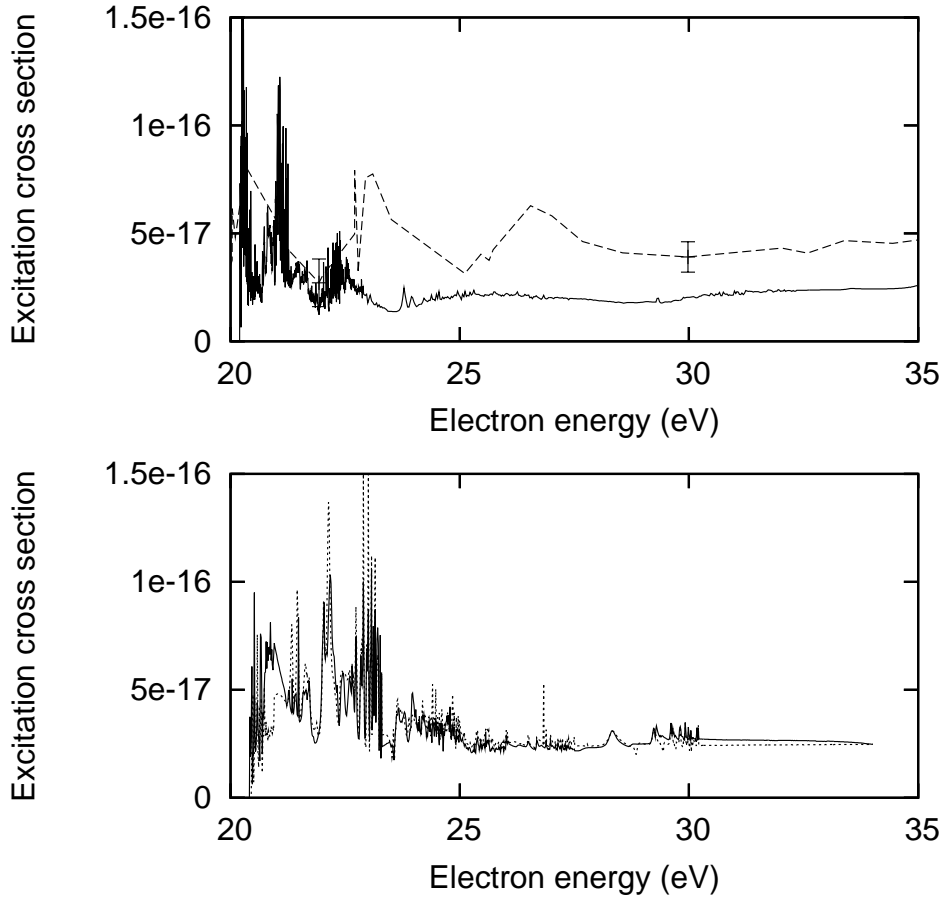
Figure 3: Excitation cross section in cm^2 for K$^+$, $^{3,1}P_1^o$ levels 3,5,8 summed: Upper plot: —, icfRM calculation; - - -, experimental points by Zapesochny et al (1986) reduced by a factor of 4. Lower plot: —, BPRM calculation; . . . ., BPRM without the $\bar{d}$ orbital.
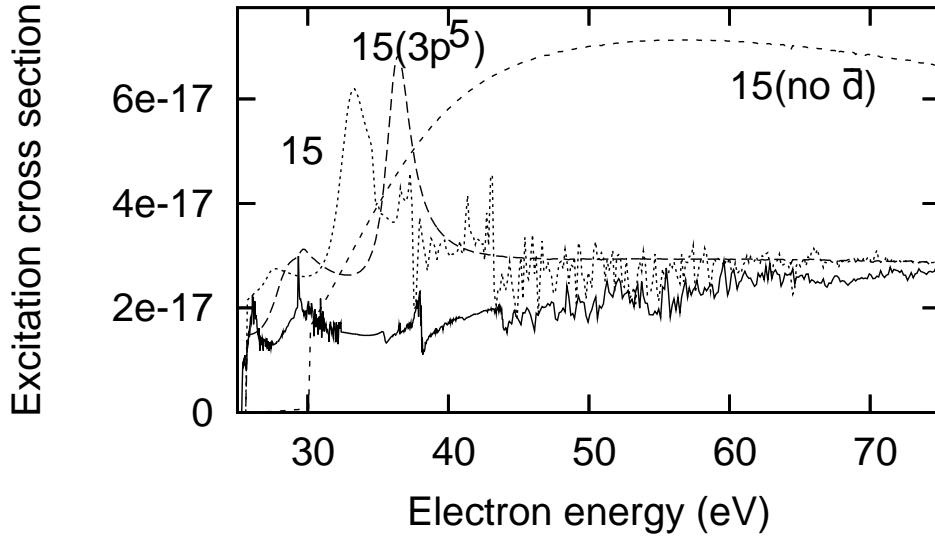
Figure 4: Excitation cross section in cm^2 for K$^+$ $3s^23p^6$ $^1S^{\text{e}} \rightarrow 3s^23p^53d$ $^1P^{\text{o}}$: —, 36 term; . . . ., 15 term; $---$, 15 term ($3p^5$ core for $N+1$ electron configurations); - - - -, 15 term (no $\bar{d}$ orbital);
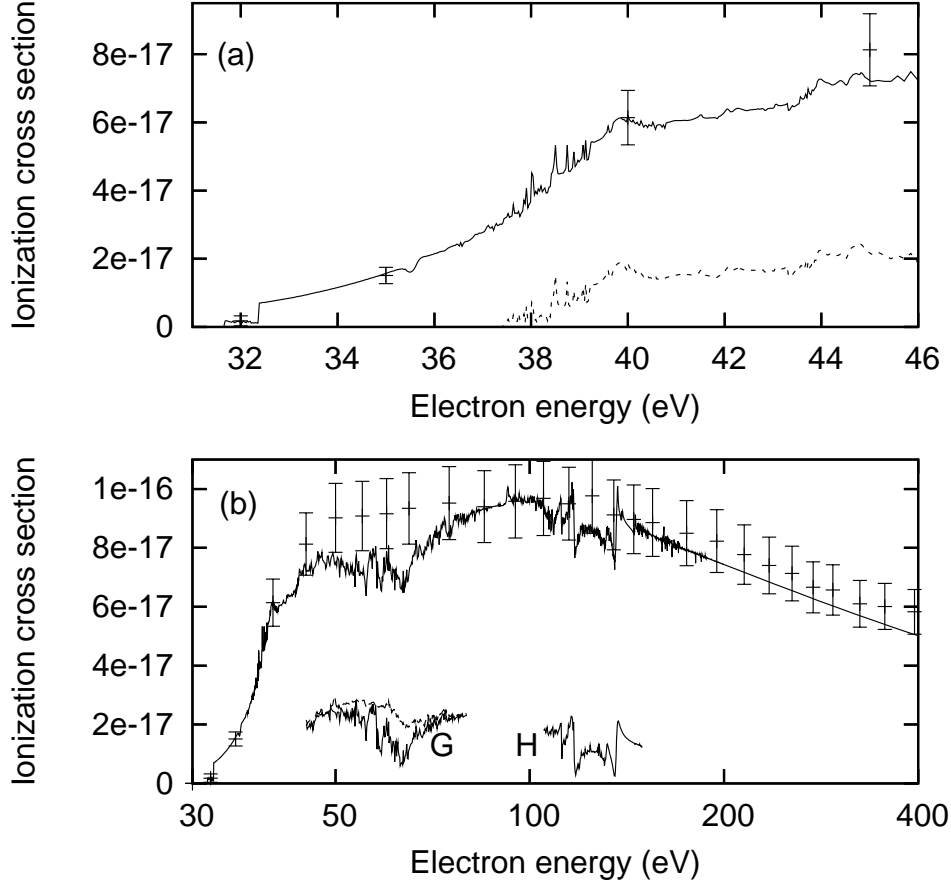
Figure 5: Electron impact ionization cross section in cm^2 for K$^+$: —, present results; - - -, innershell contribution (a); lines labelled G and H in (b) are the partial wave contributions (see text); experimental points by Hirayama (1987).
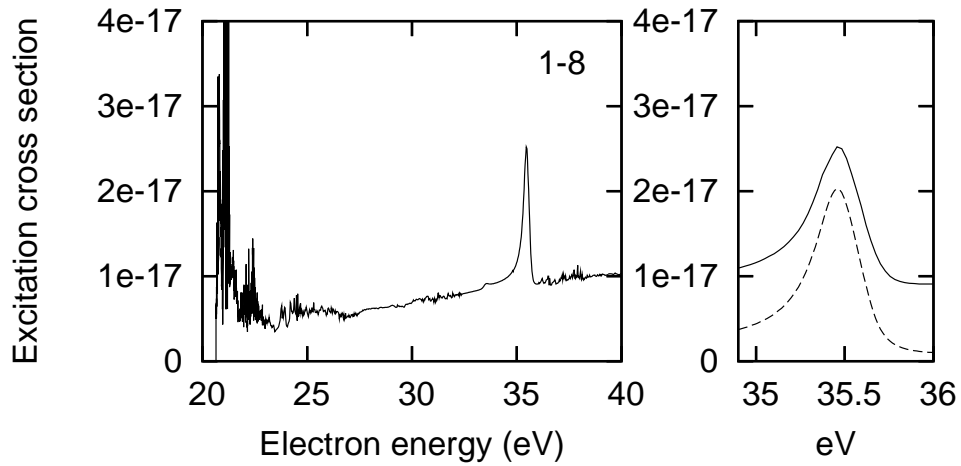

Figure 6: $3p^6\ ^1S_0^e - 3p^54s^1P_1^o$ (1–8) excitation cross section in cm^2 for K$^+$. Right plot, near the $^2D^e$ resonance at 35 eV: —, total cross section; - - -, $^2D^e$ partial wave contribution.